RESEARCH ARTICLE

INTERNATIONAL RESEARCH JOURNAL OF MULTIDISCIPLINARY TECHNOVATION

Asian Research Association

DOI: 10.54392/irjmt26426

Green Combustion Synthesis of CuO Nanoparticles Using Vitis vinifera Extract and Their Physicochemical Characterization

R. Manoranjitham [a, *], S. Sindhu Kavi [b], N. Backiyalakshmi [a], H.B. Ramalingam [c, *]

[a] Department of Science and Humanities, KGiSL Institute of Technology, Coimbatore, Tamil Nadu 641035, India
[b] Department of Physics, KPR Institute of Engineering and Technology, Coimbatore, Tamil Nadu 641407, India
[c] Department of Physics, Government Arts College, Udumalpet, 642 126, Tamil Nadu, India
* Corresponding Author Email: manoranjithamramakrishnan@gmail.com , hbramalingamhb@gmail.com
DOI: https://doi.org/10.54392/irjmt26426
Received: 09-04-2026; Revised: 08-07-2026; Accepted: 13-07-2026; Published: 30-07-2026

Abstract: Bioactive copper oxide (CuO) nanoparticles were synthesized through a combustion method using Vitis vinifera extract, and the effects of temperature on CuO calcination were shown. The structural, morphological, compositional, optical, and thermogravimetric properties were investigated. Powder X-ray diffraction confirmed the successful formation of crystalline nanoparticles with a crystallite size of 18.7 nm, and FTIR analysis confirmed the formation of the CuO phase. The morphological images revealed nanosphere-like structures, while elemental analysis confirmed the uniform distribution of Cu and O throughout the samples. TG/DTA analysis revealed the thermal stability, phase transformations, and temperature-dependent weight loss of the samples. The direct band gap energies are determined using the Tauc plot of the UV-Vis DRS data. Zeta-potential analysis was used to investigate the surface-charge characteristics and colloidal stability. These findings indicate the formation of microsphere-like assemblies composed of CuO nanoparticles. This study systematically evaluates multiple physicochemical properties to provide insight into the physicochemical characteristics that may contribute to improved gas adsorption, charge transfer, and sensing performance.

Keywords: CuO Nanoparticles, Bio-Fuel, Combustion Synthesis, Physico-Chemical Studies.

1. Introduction

Recent advances in science and technology increasingly rely on the manipulation of matter at the atomic and nanoscale levels [1]. Nanotechnology involves the design and fabrication of nanoscale materials with controlled physical and chemical characteristics [2, 3]. A nanomaterial is a material with at least one dimension in the nanometre range [4]. Nanomaterials generally have dimensions between 1 and 100 nm (10^{-9} m), and it is 100,000 times smaller than the diameter of a human hair [5]. Nanomaterials are commercialized in the form of nano powders, functionalized nanomaterials and quantum dots [6]. Nanomaterials have enhanced properties owing to their high surface area to volume ratio, electroactive property, and unique optical and electrical properties [7]. Nanomaterials were classified into zero-dimensional nanomaterials (0-D quantum dots), one-dimensional nanomaterials (1D-nanowires), two-dimensional nanomaterials (2D), three-dimensional nanomaterials (3D-bulk material) and multidimensional (combination of 1D and 2D) [8]. These dimensional classifications play a crucial role in determining properties such as surface area, electron-transport pathways, charge-transfer resistance, and quantum confinement [9]. Various capping agents and surfactants have been utilized in this setting. In recent years, plant extracts containing biomolecules such as polyphenols and terpenoids have been used as reducing and capping agents because their functional groups can coordinate with metal ions during nanoparticle synthesis [10, 11]. This incorporation may promote improved crystallinity, nanosphere-like morphology, and favourable optical properties.

Transition-metal oxide nanomaterials containing elements such as Fe, Co, Ni, Mn, Cu, and Mo have been widely reported over many years [12,13]. Transition metals are the d-block elements, and they have incompletely filled d-orbitals. In other words, they have d^1 to d^9 electrons [14]. These materials offer better structural, electrical/electronic, and magnetic properties. Transition-metal oxides can exhibit either p-type or n-type semiconducting behaviour and may possess multiple oxidation states (e.g., Fe^{2+}/Fe^{3+}, Co^{2+}/Co^{3+}, Mn^{2+}/Mn^{3+}, Ni^{2+}/Ni^{3+}), providing extensive redox chemistry [15,16]. However, when synthesized at the nanoscale, its dimensions generally range from 5 to 100 nm for nanoparticles. CuO is a p-type semiconducting material that can possess a porous morphology with a

narrow band gap in the range of 1.2–1.5 eV, which facilitates rapid charge transfer [17,18]. These result in significant excitation of electrons from the valence band to the conduction band with electron transfer flow, even at moderate and room temperatures [19]. Enhancing baseline conductivity enables measurable changes in resistance upon gas interaction. These nanomaterials have attracted considerable attention from researchers because of their diverse sensor applications.

CuO nanoparticles can be synthesized using hydrothermal [20], sol–gel [21], chemical-precipitation, and combustion methods [22]. Hydrothermal, sol–gel, and chemical-precipitation methods often require long processing times, high pressures, and multiple processing stages. To overcome these limitations, the conventional combustion method was selected due to its specific capacity to create extremely porous nanostructures with excellent crystallinity, ease of use, and quick reaction kinetics. Therefore, the combustion method is considered a cost-effective, energy-efficient, and scalable approach for synthesizing nanostructured materials suitable for high-performance electrochemical applications.

The current work focuses on the synthesis of copper oxide (CuO) nanomaterials through a facile combustion method, which facilitates their rapid reaction kinetics and enhances ability to produce highly porous nanostructures. The synthesized CuO was characterized to evaluate its structural, morphological, and optical properties using various techniques. The phase purity and crystallographic structure were analysed by X-ray diffraction (XRD), while the surface morphology and particle distribution were examined using scanning electron microscopy (SEM). Furthermore, elemental composition and spatial distribution of elements were confirmed through energy-dispersive X-ray spectroscopy (EDS) analysis. The optical absorption properties and band gap energy of the prepared CuO were evaluated using UV–visible spectroscopy. The surface charge and material stability of the synthesized material were assessed via zeta potential measurements. Based on these physicochemical characteristics, the synthesized CuO nanostructure is expected to exhibit promising properties for gas sensing applications due to its suitable band gap, high surface area, and favourable surface charge characteristics.

2. Experimental Section

2.1 Chemical Reagents

Analytical grade chemicals were used for the synthesis of copper oxide nanoparticles. Cupric nitrate trihydrate ($Cu(NO_3)_2 \cdot 3H_2O$; extra pure, 98%; ACS reagent; SRL Pvt. Ltd, India) was used without further purification. Distilled water (H_2O) was used as solvent throughout the experiment.

2.2 Preparation of *Vitis Vinefera* Extract

Fresh, commercially purchased Vitis vinifera grapes were used as the fuel source in the synthesis of copper oxide nanoparticles. The grapes were washed thoroughly with ethanol and distilled water. The fruits were crushed using agate mortar and pestle. The freshly prepared extract was filtered using Whatman filter paper to remove the fruit solids and was subsequently centrifuged at 6000 rpm for 30 minutes. The clear supernatant was collected and used as the biofuel/reducing agent for the synthesis.

2.3 Synthesis of Copper Oxide Nanoparticles

Copper oxide nanoparticles were prepared by the green extract assisted solution combustion method. 1M (12.06g) of analytical grade cupric nitrate trihydrate was dissolved in 50ml of distilled water. The solution was magnetically stirred for 60 minutes to ensure the uniform distribution of ion and complete dissolution of metal salt. The resulting homogeneous solution was then slowly added to 50 mL of Vitis vinifera extract which acts as the biofuel and reducing agent for this synthesis process. The solution was again magnetically stirred at 440 rpm for 45 minutes to facilitate the effective co-ordination between the metal ions and phytochemicals. The resultant homogenous mixture was introduced onto the pre-heated (100°C) hotplate. When the solution reached 100°C, water evaporated and gaseous species were released. Partial evaporation of the water resulted in the visible formation of a hydrogel. Further heating ignited the solution, leading to the complete combustion of the precursor mixture. The beaker was then cooled to room temperature, after which the combusted particles were collected and washed to remove impurities followed by drying at 60°C for 12h for the removal of the moisture and finally ground into a fine CuO nanoparticle powder (Scheme 1).

For the comparative study on the effect of annealing on the copper oxide nanoparticles, Separate 5 g portions of the CuO nanoparticles were placed in crucibles and were subjected to heat treatment in muffle furnace at 5°C/min heating rate for 350°C (5h) and 450°C (5h) respectively. The heat-treated samples were collected and subjected to structural, morphological, colloidal, optical, vibrational, and thermal characterization.

2.4 Characterization Instruments

The structural characterization of the prepared metal oxide nanoparticles was done by X-ray diffraction analysis, D8 Bruker Advance (Germany), under the ambient operating conditions.

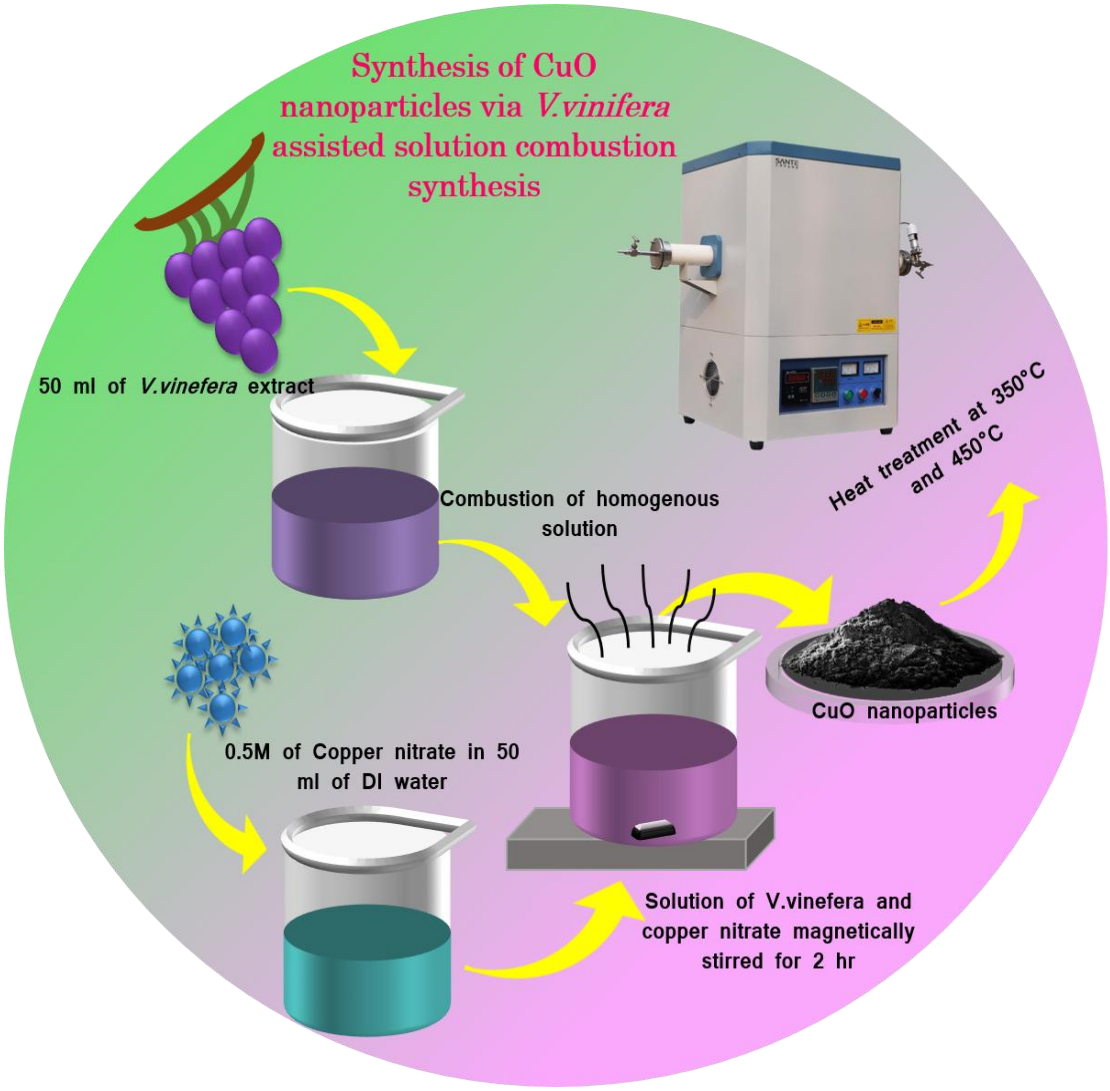

Scheme 1. Synthesis scheme for the preparation of CuO nanospheres.

The surface morphological studies and elemental composition were characterized using Field Emission Scanning Electron Microscopy (FESEM) with Energy Dispersive X-ray Spectroscopy (EDS), Carl Zeiss SIGMA 300 (Germany). The vibrational studies were carried out using Fourier Transformation Infrared analysis (FTIR), JASCO FTIR-4X, Japan with the wavenumber range of 400 cm^{-1} to 4000 cm^{-1}. The thermal stability was analyzed using Thermogravimetric / Differential Thermal analysis, Perkin Elmer, STA-800, China. The colloidal stability was investigated using zeta potential analysis, Malvern Zetasizer 1000 HS, UK. The optical properties were measured using UV-DRS (Diffuse Reflectance Spectroscopy), JASCO V67 UV-Vis-NIR spectrophotometer, Japan.

3. Results and Discussions

3.1 XRD analysis

The XRD patterns of the combustion-synthesized as-prepared CuO, CuO-350°C, and CuO-450°C samples are shown in Figure 1A–C. The XRD patterns of the as-prepared and calcined CuO nanoparticles are shown in Figure 1A-C. The diffraction peaks were observed at (2θ degree) = 32.63° (110), 35.60° (002), 38.90° (111), 48.73° (-202), 53.50° (020), 58.34° (202), 61.49° (-113), 66.4° (-311) and 68.09° (220) correspond to the hkl indices of different planes of monoclinic CuO. The diffraction patterns confirmed the formation of polycrystalline CuO with JCPDS card No. 02-1225 [23]. A predominant (111) reflection was observed in all samples. Its intensity was lower in the as-prepared sample than in the calcined samples. The results suggest that increasing the calcination temperature enhances the material's purity. The results in Table 1 show that the crystallite size decreased as the microstrain increased [24, 25], which were calculated in equation 1&2 denoted D crystallite size, β FWHM (radians), ε microstrain (dimensionless), β Full Width at Half Maximum (FWHM) of the diffraction peak in radians, and θ = Bragg diffraction angle (half of 2θ). The CuO-450°C sample exhibited more intense diffraction peaks and improved phase purity.

Crystallite Size Calculation (Scherrer Equation)

$$D = \frac{0.9\lambda}{\beta \cos\theta} \quad (1)$$

Microstrain Formula

$$\varepsilon = \frac{\beta}{4\tan\theta} \quad (2)$$

3.2 FTIR Analysis

The characteristic vibrational bands exhibited by the CuO, CuO-350°C, and CuO-450°C nanoparticles were recorded via FTIR analysis. The characteristic bands and stretching vibrations in the spectra confirm the formation of CuO phase along with the occurrence of surface functional groups. Figure 2 indicates the evolution in the FTIR spectra with respect to the heat treatment. The distinctive peaks at 583.5 cm^{-1}, 512.4 cm^{-1} and 429 cm^{-1} are the characteristics peaks of monoclinic CuO and are assigned to the M-O stretching vibrations [26, 27]. The vibrational band at 1378.65 cm-1 corresponds to the rocking vibration of C-H groups (methyl group) and the significant peak at 1039.38 cm^{-1} is consistent with previously reported C–N stretching bands of aliphatic amines. These peaks are mainly attributed to the functional groups present in the biomolecules of the grape extract assisted during the synthesis [28, 29]. As the annealing temperature increased, the intensity of these peaks decreased because of the thermal decomposition of the organic components present in the CuO samples. The weak band at 2353.14 cm^{-1} is assigned to the asymmetric stretching of CO_2 molecules adsorbed during the synthesis or present in the instrument during measurement [30]. The weak peaks in the 3500–4000 cm-1 region suggest the presence of hydroxyl groups common in green synthesis [31]. The spectra exhibit the typical M-O vibration elucidating the formation of CuO phase, and the increase in the intensity of these peaks after annealing at 450°C indicates the phase purity of the CuO 450°C sample.

3.3 Morphological Analysis

FESEM analysis was performed to examine the surface morphology of the synthesized copper oxide nanoparticles. The FESEM micrographs in Figure 3A–C illustrate the observed morphological characteristics of the CuO, CuO-350°C and CuO-450°C samples respectively. The micrographs reveal a highly porous, interconnected three-dimensional network and show how the surface morphology evolved during annealing. The CuO, as prepared sample exhibits the porous structure with irregular, agglomerated morphology. Mostly, the particles appear to be sponge like clusters with numerous voids and cavities. Figure 3B shows that annealing at 350°C caused changes in the surface morphology. The porous nature of the nanoparticles is still visible but less prominent when compared to the as prepared sample CuO. The reduction in porosity and formation of distinct grain boundaries provide evidence of initial sintering. While the morphology remains interconnected there is a notable crystallite growth and removal of residual organic matters. Meanwhile, Figure 3C exhibits a significant change in the morphology at the annealing temperature of 450°C. The samples exhibit densely packed structure with pronounced grain growth with reduced porosity. The higher temperature annealing resulted in the defined grain boundaries and reduced voids and cavities [32, 33]. The formation of porous structure with agglomerated voids and cavities for the as prepared samples is the resultant incorporation of the phytochemicals during the synthesis that serves the major role as the capping and reducing agents. Before annealing, the particles remained in agglomerated structures with poorly defined grain boundaries, whereas annealing produced well-defined crystalline particles [34]. The evolution in the morphological features with respect to the annealing process reveals the improvement in crystallinity, which may further enhance the physical and chemical properties of the copper oxide nanoparticles [35]. Additionally, the EDS spectra (Figure 3D–F) consistently confirm the presence of Cu and O elements as the primary constituents, with progressive improvement in phase purity with respect to the annealing temperature. The background signal observed in Figure 3D may indicate the presence of any residual carbon from the grape extract. The reduced background signal in Figures 3E and 3F indicates the removal of residual carbonaceous species during annealing, thereby ensuring the enhancement in phase purity and crystallinity.

Table 1. Calculated crystalline size and microstrain for the prepared sample

Sample	Crystallite Size (nm)	Microstrain
CuO As-prepared	33.7	3×10^{-3}
CuO-350 °C	26.3	3.9×10^{-3}
CuO-450 °C	18.7	5.5×10^{-3}

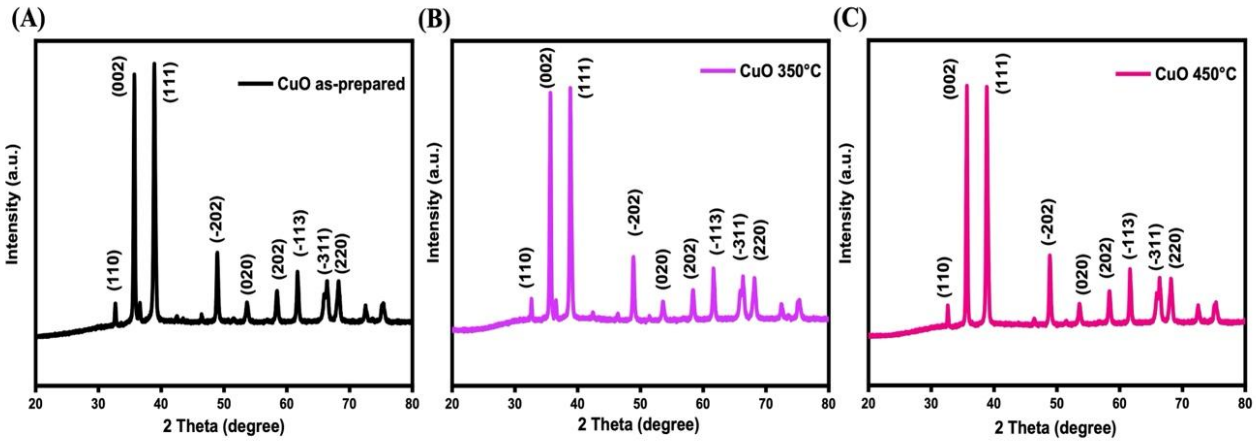

Figure 1 A-C XRD Spectrum for CuO - as-prepared sample, CuO - 350°C, and CuO - 450 °C.

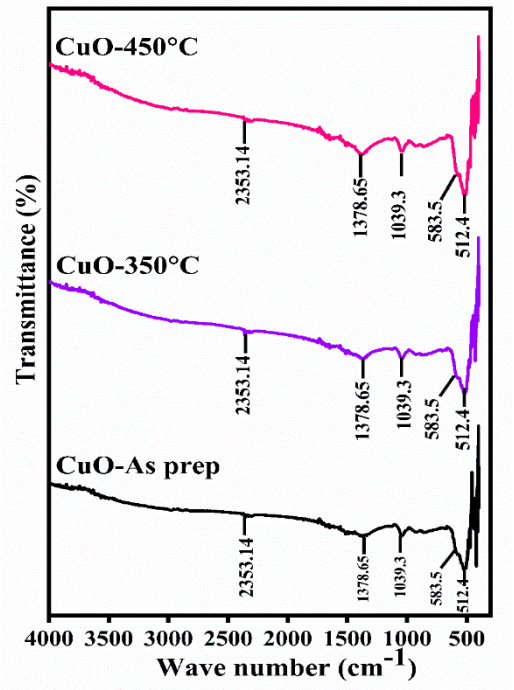

Figure 2. FTIR Spectrum for CuO - as-prepared sample, CuO - 350°C, and CuO - 450 °C.

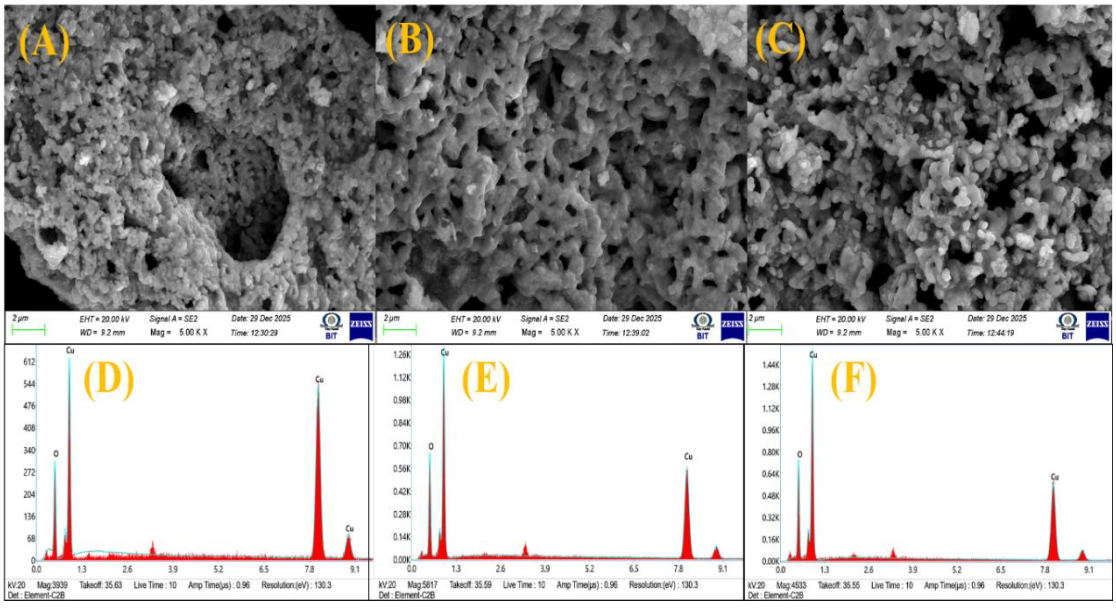

Figure 3 A-C. SEM images (D-F)for CuO - as-prepared sample, CuO - 350°C, and CuO - 4

3.4 Optical Analysis

The synthesis of CuO was conducted via the combustion method. As-prepared CuO, CuO-350 °C, and CuO-450 °C were evaluated using UV–Vis DRS in Figure 4 A-C. The direct band-gap energies were estimated by extrapolating the linear regions of the Tauc plots using Equation (3). Where E_g represents the optical band gap, hυ denotes the photon energy, A is a material-specific constant, and α is the absorption coefficient, while the parameter n defines the nature of the electronic transition [36]. The estimated band gap values were 1.318 eV for as-prepared CuO, 1.261 eV for CuO-350 °C, and 1.207 eV for CuO-450 °C, indicating a gradual decrease in the band gap energy with increasing calcination temperature [37]. This reduction in band gap may be attributed to calcination-induced improvements in crystallinity, structural modification, and the formation of defect states that influence the electronic structure, and the resulting lower charge-transfer resistance may promote stronger interactions with gas molecules of the CuO lattice.

$$(\alpha h\upsilon)^{n} = A\,(h\upsilon - Eg) \qquad (3)$$

3.5 Zeta Potential analysis

Zeta-potential analysis was used to evaluate the surface-charge characteristics and colloidal stability. The synthesised CuO nanostructures were evaluated, as shown in Figure 5A–C. Zeta potential reflects the electrostatic repulsion between dispersed particles and plays an important role in determining dispersion stability, surface interactions, and adsorption behaviour, particularly in sensor-related applications. Figure 5A presents the zeta potential distribution of the as-prepared CuO sample, which exhibits a narrow distribution centred around approximately −5.3 to −10.1 mV. This behaviour is typically associated with the presence of surface hydroxyl groups and incomplete crystallization in the as-prepared nanostructures. Upon calcination at 350°C, the CuO sample shown in Figure 5B shows a slightly shifted zeta potential value of approximately −12.1 to −15.2 mV, indicating an increase in the negative surface charge. The enhanced negative potential can be attributed to improved crystallinity and the formation of more stable surface oxygen species during thermal treatment. These negatively charged surface sites promote stronger electrostatic interactions with positively charged species, which is beneficial for adsorption and surface reaction processes.

Furthermore, the results show that calcination at 450°C produced a more pronounced negative zeta potential of approximately −18.07 to −20.01 mV, as depicted in Figure 5C. The increase in surface charge magnitude indicates improved dispersion stability and reduced particle aggregation. This enhancement can be linked to increased grain growth, improved crystal ordering, and the stabilization of oxygen-related surface functional groups on the CuO lattice.

3.6 Thermogravimetric Analysis

The Thermogravimetric / Differential Thermal Analysis (TG/DTA) has been carried out for the prepared CuO, CuO-350°C and CuO-450°C samples to comprehend their thermal stability. The exothermic and endothermic features in the TG/DTA curves indicate physical and chemical changes occurring during heating. Figure 6.a. of the as prepared sample without any prior thermal treatment exhibits a major weight loss (~66%) in five major steps. The initial weight loss of 15.5% around the temperature range of 220°C indicates the evaporation of adsorbed moisture and surface bound water. The endothermic peak around the same region confirms the process of dehydration. During the second degradation stage, the exothermic curve exhibits a major weight loss of 24.5% indicating the thermal degradation and oxidative decomposition of organic compounds of the phytochemicals in the grape extract [38]. The minor degradation events observed in stages 3–5, with weight losses of ~10.6%, ~10.1%, and ~5.9%, represent the slow decomposition of carbonaceous residues.

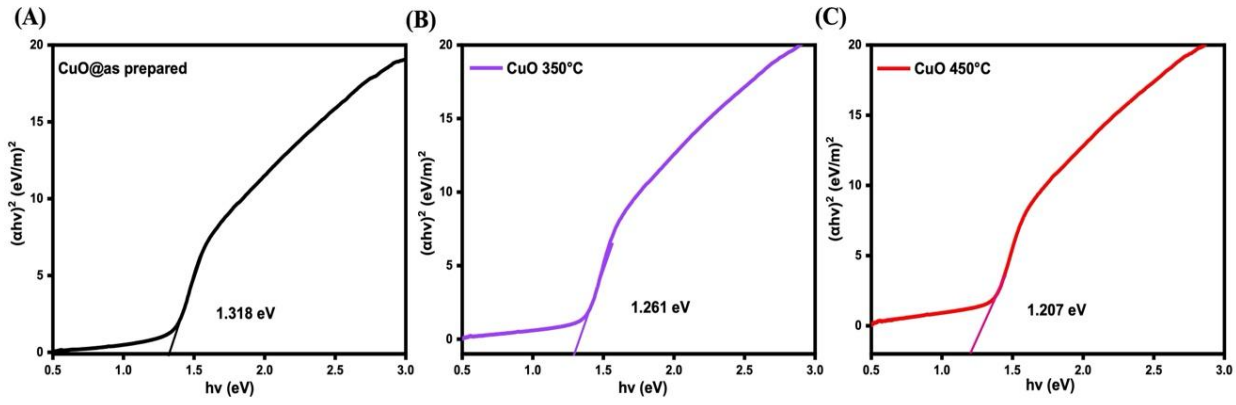

Figure 4. A-C UV direct band gap for CuO - as-prepared sample, CuO - 350°C, and CuO - 450 °C.

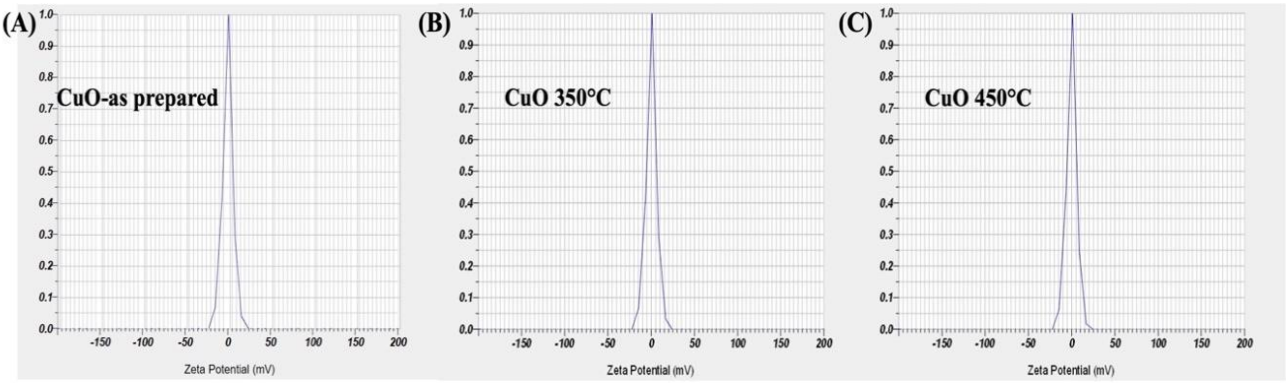

Figure 5. A-C Zeta potential for CuO - as-prepared sample, CuO - 350°C, and CuO - 450 °C

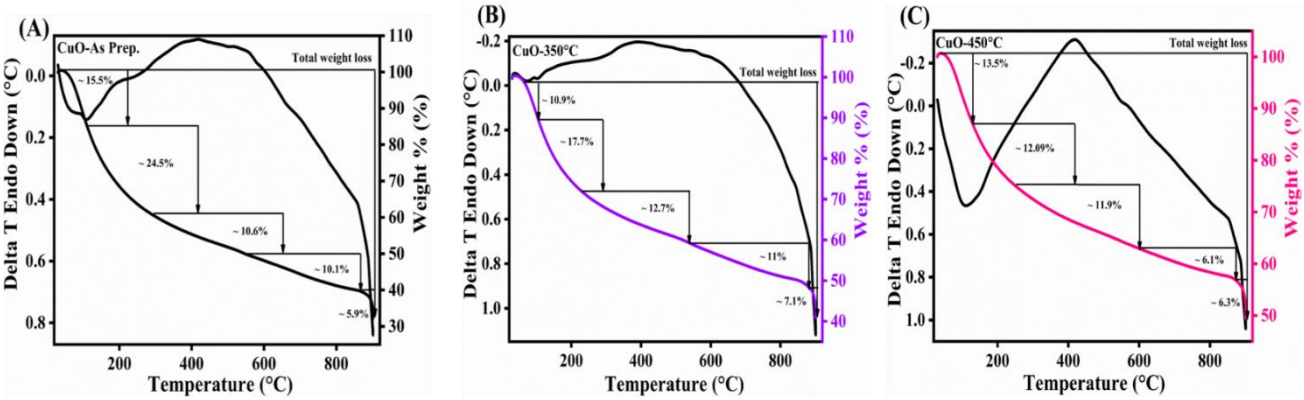

Figure 6. A-C TG/DTA analysis for CuO - as-prepared sample, CuO - 350°C, and CuO - 450 °C.

For CuO-350°C (Figure3.b) sample the total weight loss observed was ~59.4%. An initial dehydration stage occurred near 120°C, followed by a weight loss of approximately 17.7% between 150 and 300°C, indicating the decomposition of organic residues The reduced decomposition indicates that pre-annealing at 350°C led to the successful removal of the phytochemical and thereby initiating the stable oxide formation.

The CuO-450°C annealed samples demonstrated the highest thermal stability with a total weight loss of ~49.89%. After the water loss at the initial stage, the sample exhibited a 12% weight loss in the organic-residue region, which was significantly lower compared to the CuO, CuO-350°C samples, which is mainly attributed to the pre-heat treatment at 450°C, which was effective in removing the residuals from green synthesis. The minimal weight loss and higher residual mass at 900°C in comparison to the other samples indicates that the CuO-450°C sample possessed the highest phase purity and thermal stability. The comparative analysis shows that treatment at higher temperatures resulted in lower weight loss because residual organic species had already been removed. This behaviour demonstrates the importance of pre-heat treatment in removing organic capping agents and promoting the formation of a stable CuO phase.

4. Conclusion

Copper oxide nanoparticles were successfully prepared via biofuel assisted solution combustion synthesis and were subjected to thermal treatment. Changes in the physicochemical properties resulting from thermal treatment were analysed using various characterisation techniques. XRD analysis revealed increased peak intensity and a reduced crystallite size in the CuO-450°C sample. SEM micrographs showed the transformation of the porous structure into more densely packed, crystalline nanosphere-like structures as the calcination temperature increased. FTIR analysis confirmed the presence of organic compounds in the biofuel and the M–O vibration in the fingerprint region below 600 cm-1 confirmed the formation of CuO NPs. The band gap calculated from the UV-Vis DRS analysis was found to be 1.207 eV for Cu-450°C and this reduction in band-gap energy in comparison to CuO and CuO-350°C is attributed to the heat treatment. The surface-charge measurements showed that the magnitude of the surface charge and colloidal stability increased as the treatment temperature increased. Moisture loss and thermal decomposition of organic residues occurred through multiple degradation stages during TG/DTA analysis. These characterization results demonstrate that the incorporated grape extract acted effectively as both a capping and reducing agent and the importance of thermal annealing which notably improved

the physico-chemical characteristics of the prepared bio-fuel assisted CuO NPs making them promising materials for future sensing applications.

References

[1] B. Elzein, Nano Revolution: Tiny tech, big impact: How nanotechnology is driving SDGs progress. Heliyon, 10(10), (2024) e31393. https://doi.org/10.1016/j.heliyon.2024.e31393

[2] K.J. Hughes, M. Ganesan, R. Tenchov, K.A. Iyer, K. Ralhan, L.L. Diaz, R.E. Bird, J. Ivanov, Q.A. Zhou, Nanoscience in Action: Unveiling Emerging Trends in Materials and Applications. ACS Omega, 10(8), (2025) 7530–7548. https://doi.org/10.1021/acsomega.4c10929

[3] S. Malik, K. Muhammad, Y. Waheed, Nanotechnology: A Revolution in Modern Industry. Molecules, 28(2), (2023) 661. https://doi.org/10.3390/molecules28020661

[4] S.K. Murthy, Nanoparticles in modern medicine: State of the art and future challenges. International Journal of Nanomedicine, 2(2), (2007) 129-141. https://doi.org/10.2147/IJN.S2.2.129

[5] S. Bayda, M. Adeel, T. Tuccinardi, M. Cordani, F. Rizzolio, The history of nanoscience and nanotechnology: From chemical-physical applications to nanomedicine. Molecules, 25(1), (2020) 112. https://doi.org/10.3390/molecules25010112

[6] M. Rizvi, H. Gerengi, P. Gupta, Functionalization of Nanomaterials: Synthesis and Characterization. Functionalized Nanomaterials for Corrosion Mitigation: Synthesis, Characterization, and Applications, 1418, (2022) 1–26. https://doi.org/10.1021/bk-2022-1418.ch001

[7] M. Pozzi, S. Jonak Dutta, M. Kuntze, J. Bading, J.S. Rüßbült, C. Fabig, M. Langfeldt, F. Schulz, P. Horcajada, W.J. Parak, Visualization of the High Surface-to-Volume Ratio of Nanomaterials and Its Consequences. Journal of Chemical Education, 101(8), (2024) 3146–55. https://doi.org/10.1021/acs.jchemed.4c00089

[8] M.A. Darwish, W. Abd-Elaziem, A. Elsheikh, A.A. Zayed, Advancements in nanomaterials for nanosensors: A comprehensive review. Nanoscale Advances, 6(16), (2024) 4015–4046. https://doi.org/10.1039/d4na00214h

[9] J.H. Zhuang, Z. Li, Y. Liang, T. Tang, X.Y. Hu, R. Ou, Q.J. Ma, B.Y. Zhang, Y.F. Cheng, W.L. Feng, J.Z. Ou, Recent progress in two-dimensional materials: From emerging structures and synthesis approaches to electronic and sensing applications. Chemical Engineering Journal, 520, (2025) 166133. https://doi.org/10.1016/j.cej.2025.166133

[10] M. Fredsgaard, A. Fussy, G.K. Nybo, J. Papenbrock, L.S.S. Hulkko, M. Dadjoo, T. Chaturvedi, M.H. Thomsen, Polyphenols in food and food wastes: Extraction, isolation, and health applications. Food Chemistry: Molecular Sciences, 12, (2026) 100351. https://doi.org/10.1016/j.fochms.2025.100351

[11] M.H.M. Edwin, A.S. Sundara Raj, A. Mani, M. Sillanpää, S. Al-Farraj, Green synthesis of Vitis vinifera extract-appended magnesium oxide NPs for biomedical applications. Nanotechnology Reviews, 13(1), (2024) 20240048. https://doi.org/10.1515/ntrev-2024-0048

[12] D. Mladenović, M. Martins, M. Samancı, M. Charneca, A. Paul, D.M.F. Santos, A. Bayrakçeken, B. Šljukić, Low-cost transition metals (Fe, Ni, Co) on carbon aerogel for water electrolysis and supercapacitor applications. Electrochim Acta, 540, (2025) 147226. https://doi.org/10.1016/j.electacta.2025.147226

[13] Y. Yoon, P.L. Truong, D. Lee, S.H. Ko, Metal-Oxide Nanomaterials Synthesis and Applications in Flexible and Wearable Sensors. ACS Nanoscience Au, 2(2), (2021) 64–92. https://doi.org/10.1021/acsnanoscienceau.1c00029

[14] K. Sridharan, Chapter 1 - The Electromagnetic Spectrum. Spectral Methods in Transition Metal Complexes, (2016) 1–12. https://doi.org/10.1016/b978-0-12-809591-1.00001-3

[15] A. Massaro, A.B. Muñoz-Garciá, P.P. Prosini, C. Gerbaldi, M. Pavone, Unveiling Oxygen Redox Activity in P2-Type $Na_xNi_{0.25}Mn_{0.68}O_2$ High-Energy Cathode for Na-Ion Batteries. ACS Energy Letters, 6(7), (2021) 2470–2480. https://doi.org/10.1021/acsenergylett.1c01020

[16] R. Liang, Y. Du, P. Xiao, J. Cheng, S. Yuan, Y. Chen, J. Yuan, J. Chen, Transition metal oxide electrode materials for supercapacitors: A review of recent developments. Nanomaterials, 11(5), (2021) 1248. https://doi.org/10.3390/nano11051248

[17] L. Korell, S. Lauterbach, J. Timm, Wang L, Mellin M, Kundmann A, Wu Q, Tian C, Marschall R, Hofmann JP, Osterloh FE, Einert M. On the structural evolution of nanoporous optically transparent CuO photocathodes upon calcination for photoelectrochemical applications. Nanoscale Advances, 6(11), (2024) 2875–2891. https://doi.org/10.1039/d4na00199k

[18] R. Nayak, F.A. Ali, D.K. Mishra, D. Ray, V.K. Aswal, S.K. Sahoo, B..Nanda, Fabrication of CuO nanoparticle: An efficient catalyst utilized for sensing and degradation of phenol. Journal of Materials Research and Technology, 9(5), (2020) 11045–11059. https://doi.org/10.1016/j.jmrt.2020.07.100

[19] Z. Yang, N. Ghorai, S. Wu, S. He, T. Lian, Direct

and Indirect Interfacial Electron Transfer at a Plasmonic p-Cu_7S_4/CdS Heterojunction. ACS Nano, 19(1), (2025) 1547–1556. https://doi.org/10.1021/acsnano.4c14556

[20] M. Outokesh, M. Hosseinpour, S.J. Ahmadi, T. Mousavand, S. Sadjadi, W. Soltanian, Hydrothermal synthesis of CuO nanoparticles: Study on effects of operational conditions on yield, purity, and size of the nanoparticles. Industrial & Engineering Chemistry Research, 50(6), (2011) 3540-3554. https://doi.org/10.1021/ie1017089

[21] Z.R. Parekh, S.H. Chaki, A.B. Hirpara, G.H. Patel, R.M. Kannaujiya, A.J. Khimani, M.P. Deshpande, CuO nanoparticles – Synthesis by wet precipitation technique and its characterization. Physica B: Condensed Matter, 610, (2014) 412950. https://doi.org/10.1016/j.physb.2021.412950

[22] R. Prakruthi, H.N. Deepakumari, CuO nanoparticles: green combustion synthesis, applications to antioxidant, photocatalytic and sensor studies. RSC Advances, 14(39), (2024) 28703–28715. https://doi.org/10.1039/d4ra04622f

[23] Z. Dan, F. Qin, A. Makino, Y. Sugawara, I. Muto, N. Hara, Fabrication of nanoporous copper by dealloying of amorphous Ti-Cu-Ag alloys. Journal of Alloys and Compounds, 586, (2014) S134-S138. https://doi.org/10.1016/j.jallcom.2013.01.087

[24] G. Madhu, V.C. Bose, K. Maniammal, A.S. Aiswarya Raj, V. Biju, Microstrain in nanostructured nickel oxide studied using isotropic and anisotropic models. Physica B Condensed Matter, 421, (2013) 87–91. https://doi.org/10.1016/j.physb.2013.04.028

[25] A. Selvam, B.S. Bangaru, K.C. Feng, S.K.S. Babu, Z. Bayhan, A. Alshamari, C.Y. Kuo, M. Govindasamy, Fruitful design of novel synthesis of aluminium boride–f-CB nanocomposite for real-time electrochemical sensing of mercury ions in environmental water samples. Journal of Water Process Engineering, 79, (2025) 109072. https://doi.org/10.1016/j.jwpe.2025.109072

[26] A. El-Trass, H. Elshamy, I. El-Mehasseb, M. El-Kemary, CuO nanoparticles: Synthesis, characterization, optical properties and interaction with amino acids. Applied Surface Science, 258(7), (2012) 2997-3001. https://doi.org/10.1016/j.apsusc.2011.11.025

[27] K. Phiwdang, S. Suphankij, W. Mekprasart, W. Pecharapa, Synthesis of CuO nanoparticles by precipitation method using different precursors. Energy Procedia, 34, (2013) 740–745. https://doi.org/10.1016/j.egypro.2013.06.808

[28] M. Elango, M. Deepa, R. Subramanian, A. Mohamed Musthafa, Synthesis, Characterization, and Antibacterial Activity of Polyindole/Ag-CuO Nanocomposites by Reflux Condensation Method. Polymer-Plastics Technology and Engineering, 57(14), (2018) 1440–51. https://doi.org/10.1080/03602559.2017.1410832

[29] A.L.K. Venkata, S.P. Anthony, M.S. Muthuraman, Synthesis of Solanum nigrum mediated copper oxide nanoparticles and their photocatalytic dye degradation studies. Materials Research Express, 6(12), (2019) 125402. https://doi.org/10.1088/2053-1591/ab52a6

[30] M.Y. Rather, S. Sundarapandian, Facile Green Synthesis of Copper Oxide Nanoparticles and Their Rhodamine-b Dye Adsorption Property. Journal of Cluster Science, 33(3), (2022) 925-933. https://doi.org/10.1007/s10876-021-02025-4

[31] M. Kalaiyarasi, M. Nivedha, M. Mani, R. Harikrishnan, J.K. Kumar, S. Loganathan, K. Kaviyarasu, Synthesis of CuO/$NaCuSO_4$ nanocomposite using an aqueous extract of Tribulus Terrestris and their structural, optical, morphology and dielectric studies. Chemical Papers, 78, (2024) 3083–3098. https://doi.org/10.1007/s11696-023-03294-1

[32] M. Krishna, Statistical comparative analysis of microwave and conventionally annealed sol–gel derived metal oxide thin films. Journal of Materials Science: Materials in Engineering. 21(92), (2026). https://doi.org/10.1186/s40712-026-00459-0

[33] N. Parimon, M.H. Mamat, I.S. Banu, N. Vasimalai, M.K. Ahmad, A.B. Suriani, A. Mohamed, M. Rusop, Annealing temperature dependency of structural, optical and electrical characteristics of manganese-doped nickel oxide nanosheet array films for humidity sensing applications. Nanomaterials and Nanotechnology, 11, (2021). https://doi.org/10.1177/1847980420982788

[34] T. Achamo, E.A. Zereffa, H.C.A. Murthy, V.P. Ramachandran, R. Balachandran, Phyto-mediated synthesis of copper oxide nanoparticles using Artemisia abyssinica leaf extract and its antioxidant, antimicrobial and DNA binding activities. Green Chemistry Letters and Reviews, 15(3), (2022) 598-614. https://doi.org/10.1080/17518253.2022.2121620

[35] K.H. Maria, S.G. Rodriguez Bonet, M.V. Bosco, S.R. Bin Salam, D. Dhar, M. Nazzarro, O.J. Furlong, F.C. Calaza, Synthesis and Characterization of CuO Nanoparticles Using Heat Treatment Approach: Annealing Effects on Crystallite Size and Band Gap of CuO Nanoparticles. ACS Omega, 11(7), (2026) 11141–11154. https://doi.org/10.1021/acsomega.5c06800

[36] M. Toma. N. Ursulean, D. Marconi, A. Pop, Structural and optical characterization of Cu

doped ZnO thin films deposited by RF magnetron sputtering. Journal of Electrical Engineering, 70(7), (2019) 127–31. https://doi.org/10.2478/jee-2019-0054

[37] M. Zain, K.A. Yasin, S. Haq, W. Rehman, S.U. Din, S. Shujaat, A. Syed, M.K. Hossain, B.A. Paray, J. Razzokov, A. Samad, Effect of calcination temperature induced structural modifications on the photocatalytic efficacy of Fe_2O_3-ZrO_2 nanostructures: mechanochemical synthesis. RSC Advances, 14(21), (2024) 15085–15094. https://doi.org/10.1039/d4ra01944j

[38] D. Serea, N.N. Condurache, I. Aprodu, O.E. Constantin, G.E. Bahrim, N. Stănciuc, S. Stanciu, G. Rapeanu, Thermal Stability and Inhibitory Action of Red Grape Skin Phytochemicals against Enzymes Associated with Metabolic Syndrome. Antioxidants, 11(1), (2022) 118. https://doi.org/10.3390/antiox11010118

Authors Contribution Statement

R. Manoranjitham: Conceptualization, Methodology, Investigation, Data curation, Formal analysis, Writing – original draft, Visualization. S. Sindhu Kavi: Software, Validation, Resources, Formal analysis, Writing – review & editing. N. Backiyalakshmi: Methodology, Supervision, Project administration, Validation, Writing – review & editing. H.B. Ramalingam: Conceptualization, Supervision, Resources, Project administration, Writing – review & editing. All authors have read and approved the final version of the manuscript.

Funding

The authors declare that no funds, grants or any other support were received during the preparation of this manuscript.

Competing Interests

The authors declare that there are no conflicts of interest regarding the publication of this manuscript.

Data Availability

The data supporting the findings of this study can be obtained from the corresponding author upon reasonable request.

Has this article screened for similarity?

Yes